La mer 31: 79–90, 1993
Société franco-japonaise d'océanographie, Tokyo

Particle tracking in a mesoscale eddy field in an ocean*

Keiko YOKOYAMA**,*** and Kenzo TAKANO**

Abstract: Particles released instantaneously or continuously from a point source are tracked in a velocity field simulated with a prognostic, four-level, eddy resolving ocean circulation model. The model ocean extending from 25.0°N to 50.5°N in latitude and over 24.8° in longitude may be considered as a portion of the western North Pacific. Its depth is 4000m except at a ridge 1900m high. The grid size is 0.375° in latitude and 0.43° in longitude. Results with the velocity field comprising mesoscale eddies are compared with those with the time-average velocity field. For tracking over the whole ocean basin, particle trajectories are, in some cases, quite different from those governed by the time-average velocity field. For local tracking, the effect of simulated mesoscale eddies is compared with that obtained with velocity data by arrayed current meters in terms of the time required for a particle to cover a certain distance from a point source. Agreement is good.

1. Introduction

In a previous paper (YOKOYAMA and TAKANO, 1993, hereafter referred to as YT), numerical experiments were carried out on the effect of mesoscale eddies on the passive tracer dispersion in a model ocean by solving an advection-diffusion equation. The velocity data necessary to calculate the advection were supplied from a four-level, eddy resolving general circulation model driven by a surface wind stress and a surface heat flux.

The model ocean extends from 25.0°N to 50.0°N in latitude and over 24.8° in longitude, and is 4000m deep except at a ridge 1900m high. Its geometry is a rough copy of a portion of the western North Pacific. The grid size is 0.43° in longitude and 0.375° in latitude. The horizontal components of velocity are defined at depths of 80, 400, 1600 and 2600m. The vertical component of velocity is defined at depths of 240, 1000 and 2100m. The simulated velocity data are available for about 80 years.

The present paper describes tracking of particles over the whole ocean basin and a local area of limited extent. As YT, this is done in the framework of a preoperational survey for the ocean bottom disposal of low-level radioactive wastes, together with a long term current measurement from 1978 to 1985.

* Received March 1, 1993
** School of Environmental Sciences, University of Tsukuba, Tsukuba, Ibaraki-ken 305 Japan
*** Present affiliation: NTT Data Communications Systems Corporation, Toranomon, Toyo 105 Japan

2. Numerical experiments

Three experiments are carried out; one is for the basin-wide tracking, and the others for local tracking over a limited area. Particles released instantaneously or continuously are assumed to move with surrounding water and tracked in the given velocity field.

The particle location $x(t+\Delta t)$ and $y(t+\Delta t)$ is determined from the location $x(t)$, $y(t)$ at time t by an upcurrent scheme as

$$x(t+\Delta t)=x(t)+u(x(t), y(t))\,\Delta t,$$
$$y(t+\Delta t)=y(t)+v(x(t), y(t))\,\Delta t,$$

where Δt is the time step, u and v are the horizontal (x-, y-) components of velocity at time t. Diffusion is neglected.

2.1 Basin-wide tracking

A similar experiment was done in a smaller ocean in a previous paper (TAKANO and MATSUYAMA, 1979).

The particle trajectory is shown by its three projections on the horizontal, vertical-meridional and vertical-zonal plane.

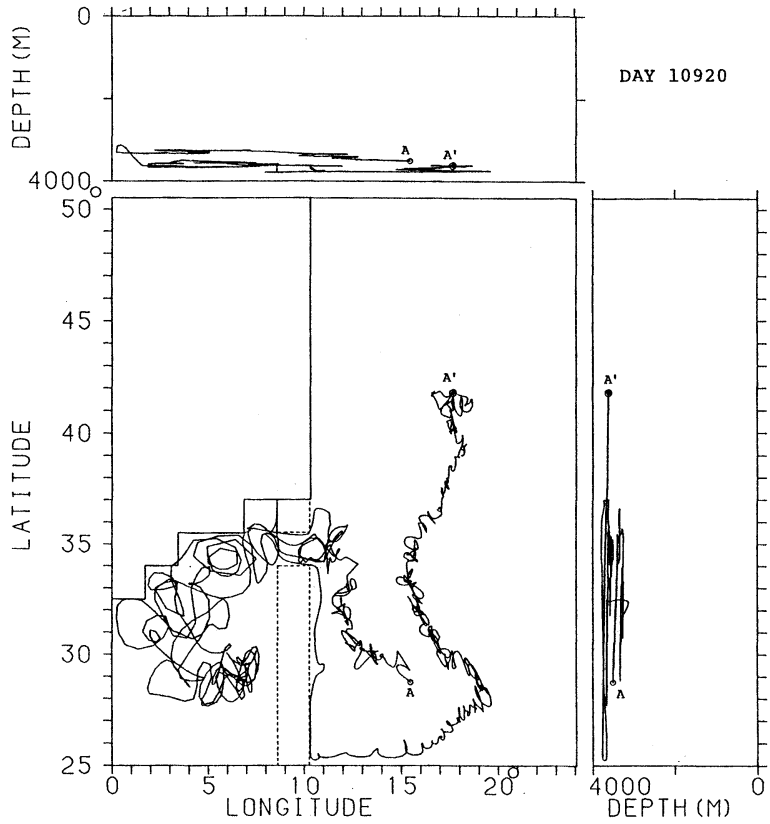

Fig. 1. An example of basin-wide tracking of a particle released from a point source A 3510m deep. The end point is A'. The projection of its trajectory on a horizontal plane is shown on the lower left, the projection on a meridional plane on the lower right, and the projection on a zonal plane on the upper left.

An example is given in Fig.1 for an instantaneous release from a point A. The location of A might correspond with the location of an area proposed by the Japanese government for the ocean bottom disposal of low-level radioactive wastes, which is centered at 30°N, 147°E, about 400km east of the Izu-Ogasawara Ridge and about 500km south of the Kuroshio Extension. One particle released from a point source A at a depth of 3510m is advected in a mesoscale eddy field and reaches a point A' at day 10920 after the release. The successive particle location is calculated by a time step of 12 hours. Since the velocity field supplied from the general circulation model is available every 2.5 days, the velocity field is updated by interpolation every 12 hours. Also linear interpolation in the zonal, meridional and vertical direction applies to get the velocity at a given location. All the successive locations determined at intervals of 5 days are used for plotting.

The particle always remains deeper than 3085m. It goes to the west of the ridge through the gap, and then comes back to the east of the ridge. To the east of the ridge, fluctuations of scales of several tens of kilometers are pronounced, except along the eastern side of the ridge where the mesoscale eddies are not active as shown in YT. To the west of the ridge, such small scale fluctuations are not so remarkable, but scales of 200 to 400km are clearly seen.

Figure 2 gives the trajectory for the same 10920 days in the velocity field averaged over 80 years. Its trajectory is confined into the east of the ridge, where it almost coincides with the trajectory in Fig.1 if the latter is smoothed out. Trajectories of five particles released from A every 25 days are shown in Fig.3 at day 10920

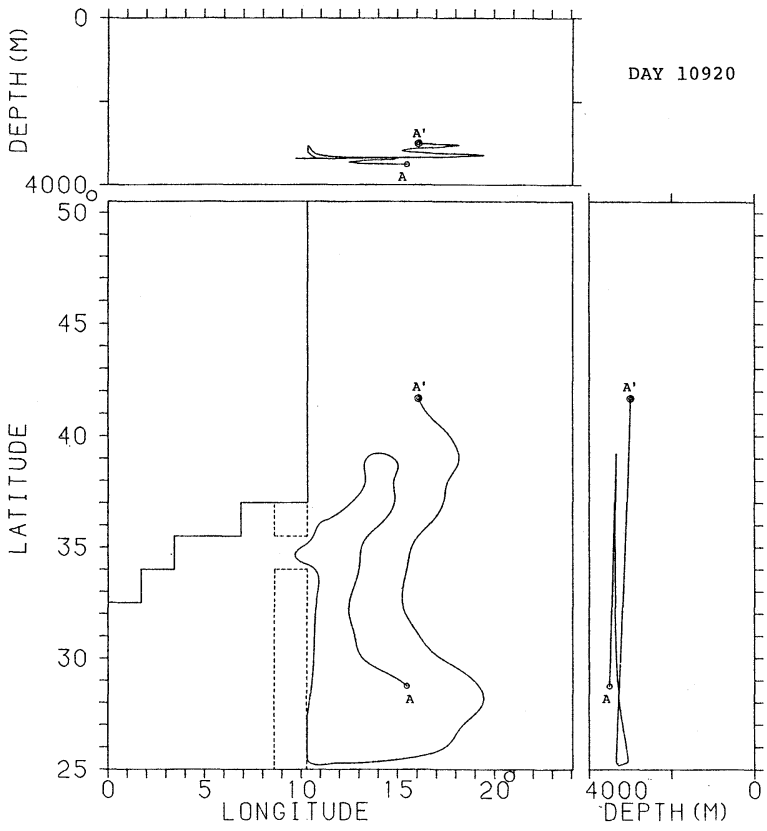

Fig. 2. Same as Fig.1 except for the time-average velocity field.

after the release of the first particle. Two of the five particles including the particle drawn in Fig.1 go to the west of the ridge through the gap. The particle is admitted into the west if mesoscale eddies timely work at the gap. Small scale fluctuations are weak not only in the west of the ridge but also in the notrhern region, which is common to the other experiments of release in the deep layer. Figure 4 shows trajectories of three particles simultaneously released at a depth of 50m. Small scale fluctuations are not so remarkable, because the mesoscale eddies are weaker relatively to the time-average in upper layers than in lower layers, and the greater part of trajectories remain in upper layers. Although they finally penetrate into deeper layers from the northern region, their trajectories are entangled in upper layers, especially in the western region, and not straightforward to the deep layer.

The extent of dispersion depends on the location of the point source, particularly on its depth. If particles are released at a shallower depth, they are dispersed wider, particularly in the vertical, governed by stronger currents. In the case where the source is deeper than the top of the ridge (2100m deep), the ridge effectively obstructs the dispersion between its eastern and western sides; particles approaching the ridge can not get over it and the gap is too narrow.

2.2 Local tracking

Instantaneous release Particles are tracked for an extent of several tens to several hundreds of kilometers. Two-dimensional instead of three-dimensional dispersion is dealt with, because the dispersion takes place in a small area and the horizontal component of the velocity is much greater than its vertical component.

A rectangular frame is set up near the bottom. Particles are released from a point source in this frame, and then advected in either the mesoscale eddy field or the time-average veloc-

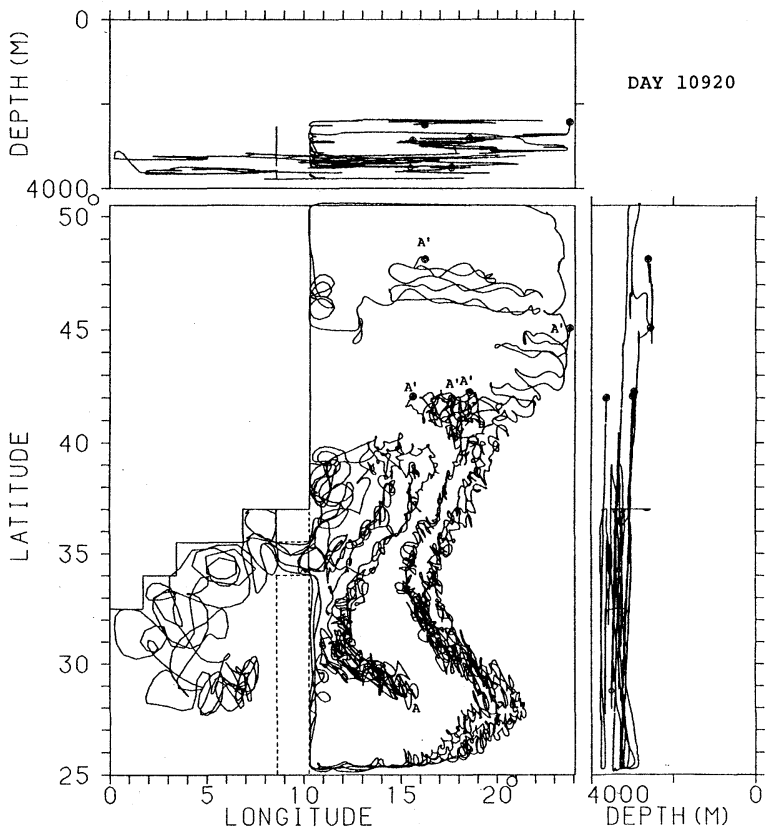

Fig. 3. Trajectories of five particles released from A every 25 days. The locations 10920 days after the release of the first particle are denoted by A'.

ity field, and finally flow out of the frame. The residence time is defined as the time elapsed from the release to flowing out, and denoted by *Re* when the particles are advected in the mesoscale eddy field, and by *Ra* when advected in the time-average velocity field. Particles once flowing out of the frame may flow back into the frame later on, but such a return is ignored in calculating *Re* and *Ra*. The residence time, either *Re* or *Ra*, depends on the frame size as well as the flow velocity. Ten frames of different size are set up at A shown in Fig.1. The side length L is about 42, 84, 167, 250, 290, 330, 380, 420, 470 and 520km.

If the side length of the frame is much longer than the predominant space scale L^* of velocity fluctuations, the velocity fluctuations have no important effect on the residence time, which is determined primarily by the time-average velocity. If the side length is comparable to L^*, the residence time will be approximately proportional to the frame area L^2. If the side length is little shorter, it will be proportional to L^n $(1<n<2)$. If the side length is much shorter, it will be proportional to L. The mesoscale eddies are the most important fluctuation component. Therefore, if the frame size is comparable to the scale of mesoscale eddies, then

$$Re \propto L^2, \quad Ra \propto L, \quad Re/Ra \propto L,$$

and, if the frame size is a little smaller than the scale of mesoscale eddies, then

$$Re/Ra \propto L^{n-1}.$$

Continuous release One particle is released every 25 days for 3.6 years. In total, fifty-one particles are released. The velocity data for these 3.6 years are arbitrarily chosen among the available data for 79.2 years. There is almost no secular variation in the data. For example,

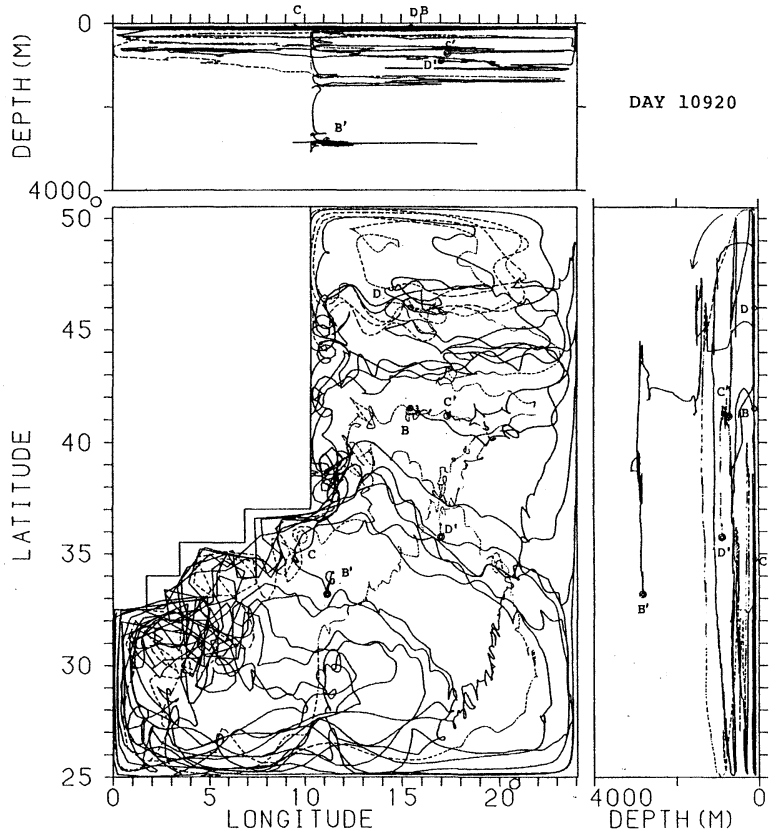

Fig. 4. Trajectories of three particles released from point sources B, C and D (depth: 50m). Double open circles B', C' and D' denote their locations at day 10920.

the simulated data for 79.2 years are divided into three parts for an equal period of 26.4 years. The time-average of u at a depth of 2600 m at Point A in Fig. 1 is −3.7 cm/s for the first part, −4.0 cm/s for the second part and −3.9 cm/sfor the last part. The time-average of v is 2.9 cm/s, 3.0 cm/s and 3.0 cm/s, respectively. There is almost no difference in the power spectra between these three parts, either.

Figure 5 shows stick diagrams of the deviations from the time-averages of the barotropic and baroclinic components at Point A for a period of 2580 days arbitrarily chosen. Although fluctuations of periods of some hundreds of days clearly appear in both components, those of the barotropic component are more energetic. The time-averages of the eastward and northward barotropic component are −0.48 cm/s and −0.23 cm/s, respectively, which are much smaller than the deviations. Those of the baroclinic component are 0.04 cm/s, −2.2 cm/s at a depth of 80 m, −0.50 cm/s, −0.61 cm/s at a depth of 400 m, 0.35 cm/s, −0.05 cm/s at a depth of 1600 m, and −0.01cm/s, 0.55 cm/s at a depth of 2600 m, which are smaller than the deviations. The time scales of the barotropic component are considerably shorter than those of the baroclinic component. The fluctuation of the baroclinic component at a depth of 80 m is well correlated with that at a depth of 400 m. The fluctuation at a depth of 1600 m looks to be correlated with that at a depth of 2600 m, but the correlations between fluctuations at the upper two layers and lower two layers are poor, as already pointed out in YT.

Figure 6 shows power spectra calculated with 79.2-year data at a depth of 2600m at A. There are predominant periods of about 100 days.

An example of the trajectories of 51 particles is shown in Fig. 7 for a frame of about 84km ×

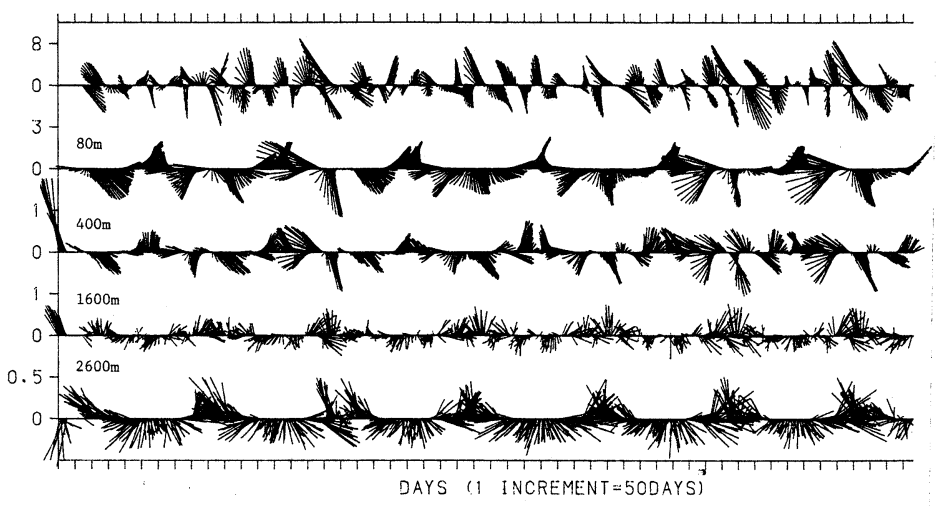

Fig. 5. Stick diagrams of the deviations of the barotropic (top diagram) and baroclinic (lower diagram) components of velocity from their time-averages at A. Units of numbers in ordinate: cm/s.

84km. The velocity data are different from those drawn in Fig. 5. The time elapsed from the first and last particle release is 3.6 years, which is long compared with the time scale of the mesoscale eddies. Trajectories in a larger square are shown in Fig. 8. The velocity data are the same as those used in Fig. 7. As expected, the trajectory has a tendency to be a curve rather than a straight line with increasing frame size.

If the time-average velocity is used, all the trajectories become nearly straight lines irrespective of the frame size.

Figure 9 gives the ratio Re/Ra for ten frames of different size of which the side length is represented in terms of the number of grid boxes N. Since the grid size is 0.375° in latitude and 0.43° in longitude, an increment of N is equivalent to about 40km. Two periods are arbitrarily chosen from 79.2-year time-series of velocity: one is the period used for Fig. 8 and the other is a period 9030 days later. Fifty-one particles are released in each data set. The average of 51 values for Re/Ra in the former are shown by open circles and the averages in the latter by solid circles. The dispersion is indicated by a line segment for each. Two results are should have been exactly at $N=1, 2, , 16, 18$, though both are a little spaced only for the sake of presentation. The upper panel is the result in the velocity field obtained with the free-slip condition at the lateral boundary, and the lower panel the result with the non-slip boundary condition.

For N smaller than 6 (about 240km), the vertical component of the velocity and the variation of the zonal side length with latitude are neglected. Although the dispersion range shown by a line segment is fairly wide, it gets narrower with increasing frame size. The average of the 51 values increases almost in proportion with the frame size for N smaller than 8 or 10 (320km to 400km), and becomes 0.8 to 0.9 irrespective of the frame size for larger frame sizes, as expected from the above simple analysis.

Table 1 summarizes the results shown in Fig. 9. The average residence time Re and Ra are tabulated with the ratio Re/Ra for ten frames of different size. The ratio Re/Ra for a given frame does almost not depend on the dynamical condition at the lateral boundary.

According to the above analysis, we have, with a constant of proportionality, d, for the frames of $N=1$ and 2,

$0.18=d\times 1^{n-1}$, $0.27=d\times 2^{n-1}$, which give
$1.5=2^{n-1}$, so that $n=1.6$ for the free-slip condition, and
$0.17=d\times 1^{n-1}$, $0.22=d\times 2^{n-1}$, which give

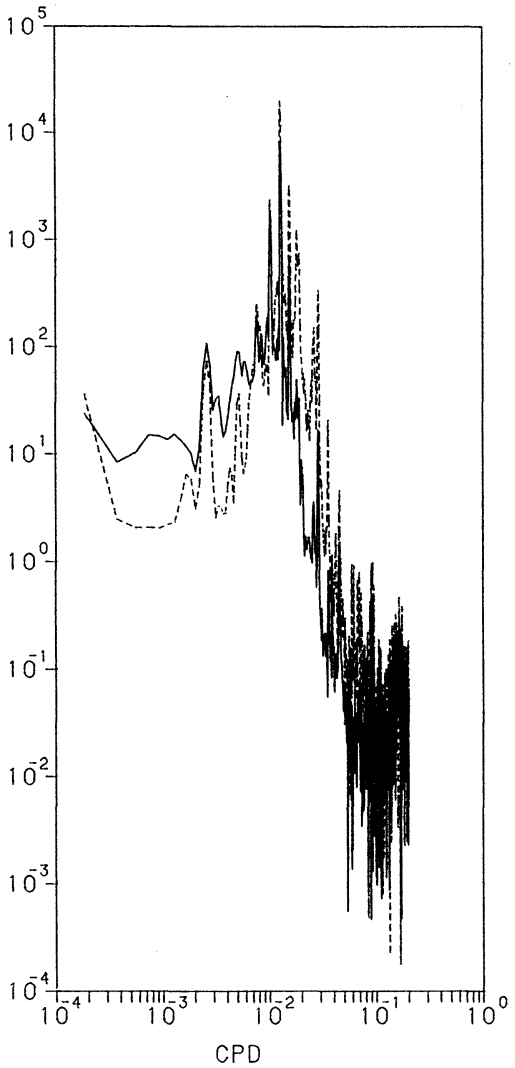

Fig. 6. Power spectra of the eastward (solid curve) and northward (broken curve) component of velocity at a depth of 2600m at A.

$1.3=2^{n-1}$, so that $n=1.4$ for the non-slip condition.

Two values 1.6 and 1.4 will be discussed later in the light of tracking experiment with observed data.

3. Particle tracking by observed velocity data

Seven-year current measurements were done around 30° N, 147° E (IMAWAKI and TAKANO, 1982; Atomic Energy Management Center, 1986).

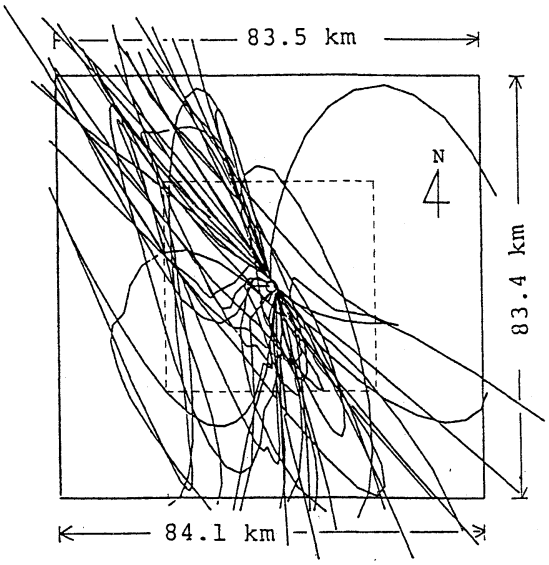

Fig. 7. Trajectories of 51 particles released every 25 days in a frame of about 84km × 83km. The side length of the inner frame is about 42km.

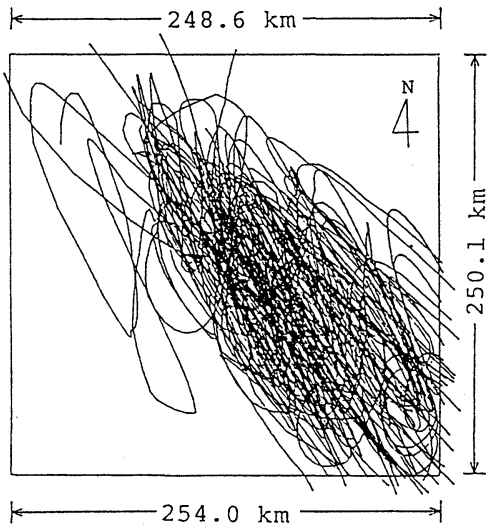

Fig. 8. Same as Fig.7 except for a frame of about 250km × 250km.

Two extensive measurements were done, the first one with a five-current meter array from May 1983 to October 1983 and the second one with an eleven-current meter array from July 1984 to July 1985, of which the locations are shown in Fig.10. Hourly data are obtained in both measurements.

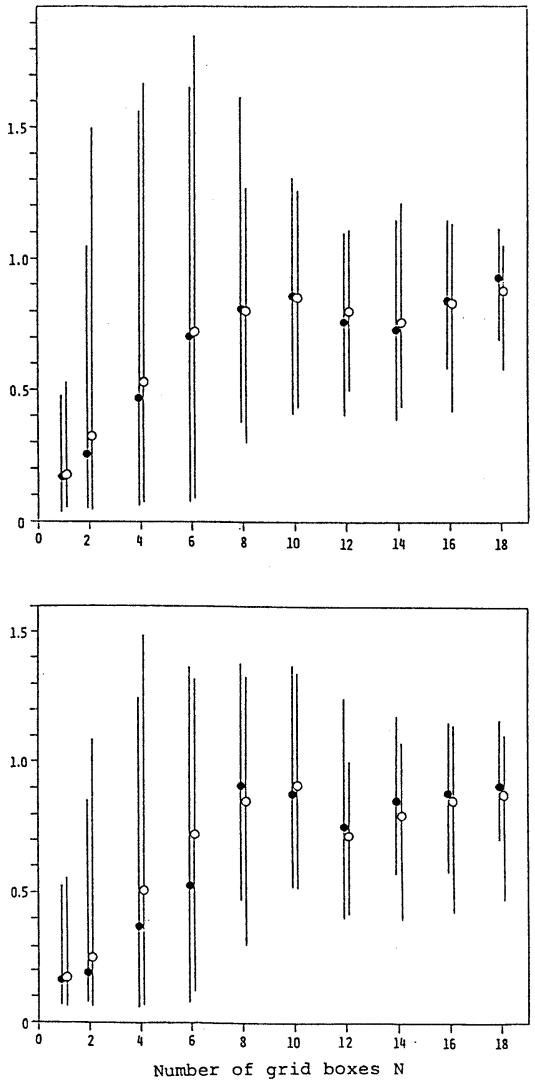

Fig. 9. Ratio Re/Ra. The ranges of dispersion are shown by line segments with the averages denoted by open circles (first period) and solid circles (second period). Velocity field with the free-slip condition (upper panel) and the non-slip condition (lower panel) at the lateral boundary.

Fluctuations of hourly data with periods around one day are apparent at all the stations, but their phases are different from each other, indicating that the scales of these fluctuations are mostly small compared with the spacing between two neighboring stations. This will be also shown later by particle trajectories. Mesoscale eddies clearly appear on the daily average. Contrary to hourly data, fluctuations are almost in phase over all the stations.

The diurnal, semi-diurnal tides and/or inertia oscillations appear in high frequency ranges in power spectra. The theoretical inertia periods at the mooring sites (29°35.2′ N to 30°15.6′ N) are 23.81 to 24.30 hours. The mesoscale eddies are predominant in lower frequencies.

3.1 Tracking with data from July 1984 to July 1985

It is assumed that one particle is released every five days from a point source located at the center of the frame of 70.7km × 70.7km shown by solid lines in Fig.10. Particles are advected by the daily mean velocity at a depth of 4000m. The total number of particles released during the observation period is 67. Letters B, V, N and R at the four corners of the frame in Fig. 11 refer to the stations shown in Fig.10. The trajectories are more scattered than those in Fig. 7. The time elapsed from the release of the first particle to the release of the last particle is 1250 days in Fig. 7, which is much longer than 330 days in Fig. 11. The number of particles released (51 in Fig.7) is only a little less than 67 in Fig.11. The trajectories are, however, much more dispersed in almost all directions than in Fig.7. A possible interpretation of this difference in pattern is that the simulated velocity field has no small scale components; the shortest resolvable wavelength is twice the grid size (about 80km).

Figures 12 and 13 give trajectories of particles instantaneously and simultaneously released. Particles in Fig.12 are released 3840 hours after the beginning of the measurement. Particles in Fig.13 are released 40 days after particles drawn in Fig.12. Hourly data are used instead of daily mean velocities. Small loops showing clockwise rotation reflect diurnal, semidiurnal tides and inertial oscillations, which are clearly seen in stick diagrams by the hourly data and power spectra (not shown here). In Fig. 12 four particles flow to the northeast, while one particle flows to the southwest. In Fig.13, five particles flow almost in the same direction (to the west-northwest). The residence time is much longer in Fig.12 than in Fig.13, which also indicates variability of the current for a period of 40

Table 1. Average residence time *Re*, *Ra* (in days) and ratio *Re*/*Ra* for ten frames of different size. The side length of frame is represented by the number of grid boxes *N*. The velocity fields used for the upper and lower panels (a and b) are obtained with the free-slip and non-slip lateral boundary condition, respectively.

	N	1	2	4	6	8	10	12	14	16	18
	Re	11.0	27.3	95.1	196	304	423	527	690	835	989
(a)	*Ra*	62.5	100.0	190.0	275	377	492	701	927	1000	1093
	Re/*Ra*	0.18	0.27	0.50	0.71	0.81	0.86	0.75	0.74	0.84	0.90
	Re	11.8	22.9	86.2	181	347	461	613	768	885	991
(b)	*Ra*	70.0	105.0	200.0	288	392	511	829	924	1015	1102
	Re/*Ra*	0.17	0.22	0.43	0.63	0.89	0.90	0.74	0.83	0.87	0.90

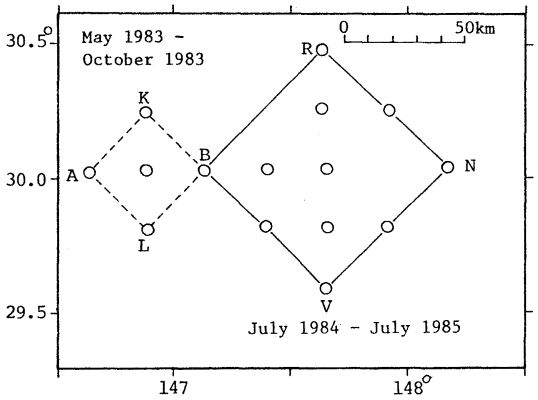

Fig. 10. Five-current meter array and eleven-current meter array at a proposed area for the ocean bottom disposal of low-level radio-active wastes. Also are shown rectangular frames used for particle tracking experiments.

days.

3.2 Tracking with data from May 1983 to October 1983

Figures 14 to 16 are drawn with data from May to October 1983. The period of measurement is shorter, so that only 30 particles are released. The time elapsed from the release of the first particle to the release of the last particle is 145 days, while it is 125 days for the numerical experiments. As in Fig. 11, the trajectories in Fig. 14 are scattered in almost all directions compared with Fig. 7 (inner frame). Since the frame size is much smaller than the mesoscale eddies, most of the trajectories are straight lines rather than curved lines except small loops by tidal and inertia oscillations. These features are also seen in Figs. 15 and 16 for an

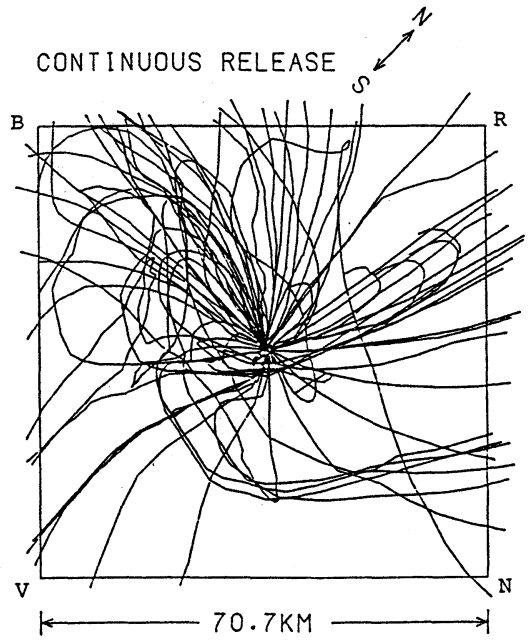

Fig. 11. Trajectories of 67 particles released every five days in the observed velocity field.

instantaneous and simultaneous release. Particles in Fig. 15 are released just at the beginning of the measurement. Patricles in Fig. 16 are released 40 days later. Trajectories in both figures are nearly straight compared with those in Figs. 12 and 13.

The trajectories in the time-average velocity field rotate clockwise from july 1984 to July 1985, but anticlockwise from May to October 1983, which indicates that the velocity field, though averaged over the whole period of the measurement, significantly changes from one measurement to another.

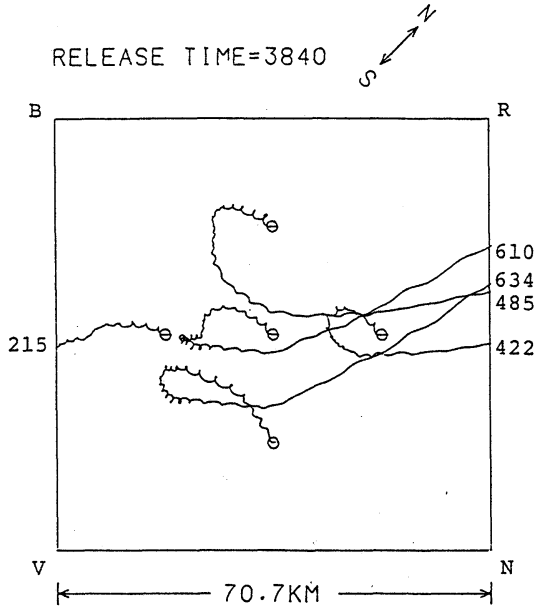

Fig. 12. Trjectories of five particles instantaneously and simultaneously released from five point sources. A numeral at the end of each trajectory denotes the residence time in hours.

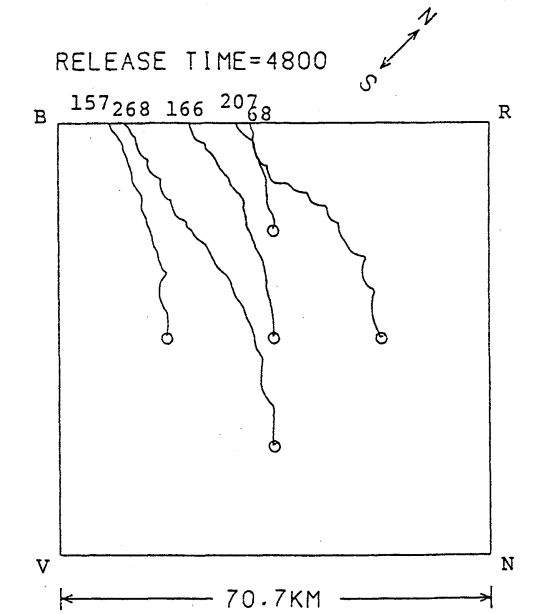

Fig. 13. Same as Fig.12 except for another release time (40 days after those in Fig.12).

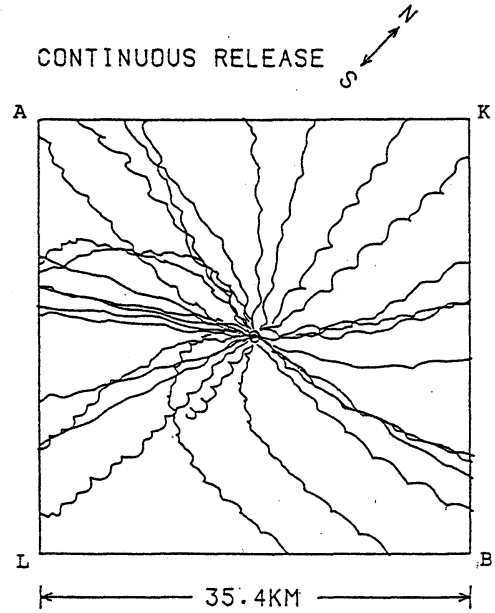

Fig. 14. Trajectories of 31 particles released every five days from May to October 1983.

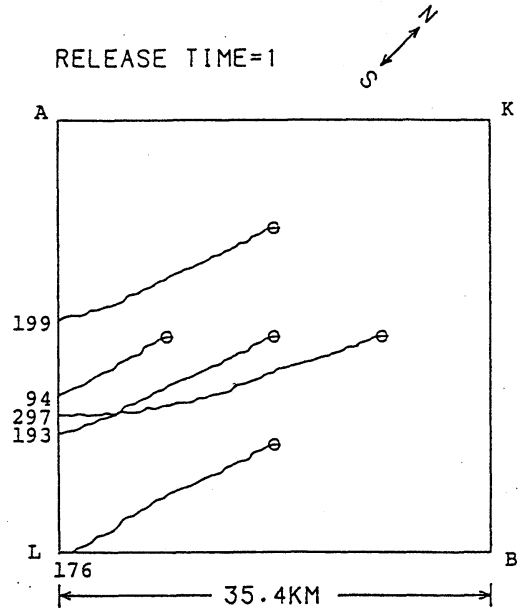

Fig. 15. Trajectories of five particles instantaneously and simultaneously released from five point sources. A numeral at the end of each trajectory denotes the residence time in hours.

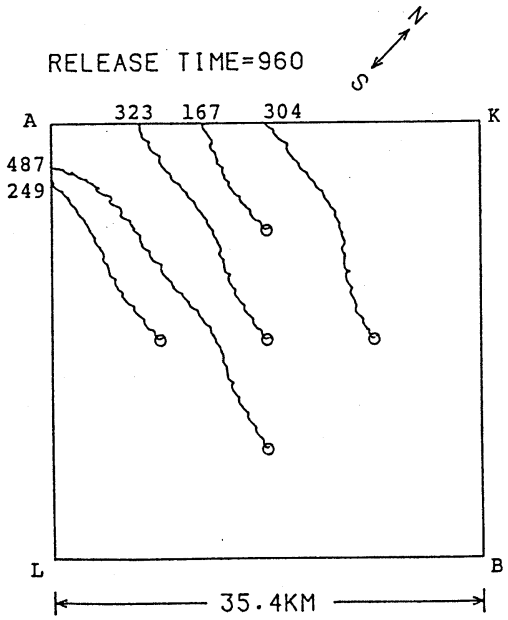

Fig. 16. Same as Fig. 15 except for another release time (40 days after those in Fig.15).

Table 2 tabulates the residence times of 30 and 67 particles. The average of ratio Re/Ra is 0.22 and 0.33, respectively, though the dispersion is fairly large. As mentioned earlier, this ratio should be proportional to L^{n-1}. From $(70.7/35.4)^{n-1}=0.33/0.22$, it follows $n=1.6$, which is equal to the value for interpreting results of the numerical experiment (with the free-slip boundary condition) for frames of size comparable with that set up by the current meter array. The value n depends on both frame size and scale of the velocity field structure, Since the frame size concerned is not so different between the numerical experiment and the observation, the agreement of the n-value indicates the statistical nature of the simulated velocity field is close to the observed one in this aspect.

4. Remarks

A previous paper (YT) shows the mesoscale eddies considerably enhance the basin-wide dispersion, especially in the vertical direction, and a small gap of the ridge cannot be an effective pathway. The present paper shows that timely intervention of the mesoscale eddies at the gap is of importance in determining the basin-wide trajectory of a particle.

Table 2. Maximum, minimum and average of residence time Re in the observed mesoscale eddy field, Ra in the average field and ratio Re/Ra. Both Re and Ra in days.

		May-Oct. 1983	July 1984-July 1985
Square(km^2)		35.4×35.4	70.0×70.0
Re	Max	16.0	41.0
	min	3.0	4.0
	mean	6.5	16.0
Ra		29.9	48.7
Re/Ra		0.22	0.33

As to the relationship between the residence time and the frame size, results of tracking experiments with the observed velocity data agree well with those calculated with the simulated velocity.

Circular frames might be more suitable for the calculation of the residence time than square frames when the point source is located at the center. The latters are, however, chosen for simplicity of calculation. The results will not change much if circular frames are set up.

A short experiment on streakiness was also attempted in the course of the present study for examining whether a spot of dye spreads into a cloud or into a number of streaks separated by clear water. In view of its importance in dispersion process, streakiness has been one of the recent topics (for example, HAIDVOGEL, 1982). No streaks were developed. However, further careful experiments are needed for understanding the behavior of an instantaneous release of dye in a mesoscale eddy field in terms of streakiness, which is of practical importance in ocean disposal of industrial wastes.

References

Atomic Energy Management Center (1985): Report of a preoperational survey of a proposed area for ocean disposal of radioactive wastes ——low-frequency water motion——. 270pp. (in Japanese)

HAIDVOGEL, D. (1982): On the feasibility of particle tracking in Eulerian ocean models. Ocean modelling, (45), 4–9. (unpublished manuscript)

IMAWAKI, S. and K.TAKANO (1982): Low-frequency eddy kinetic energy spectrum in the deep western North Pacific. Science, **216**, 1407–1408.

TAKANO, K. et S. MATSUYAMA (1979): Dispersion de polluants d'une source au fond porfond par des tourbillons â échelle intermédiaire. Radioécologie marine, Compte rendu du troisième Colloque de l'AEN, 117–127.

YOKOYAMA, K. and K.TAKANO (1993): Dispersion of passive tracers in an oceanic mesoscale eddy field. La mer, **31**, 59–78.

中規模うずを含む海での粒子の追跡

横山恵子・高野健三

要旨：中規模うずを含む流れの中の粒子を追跡する。流速は，4層の，うず分解循環モデルから与えられる。海は緯度方向には25.0°Nから50.5°Nまでひろがる。経度方向のひろがりは24.8°である。海の深さは，南北方向に走る海嶺（海底の高さは1900m）を除いて一定（4000m）であり，北西太平洋の一部に似た形になっている。うずを含む流速場と時間平均をとってうずを除いた流速場を使う。(i) 約30年にわたる追跡実験と，(ii) 数日から3年程度までの追跡実験，を行う。(i) では，平均流速を使うと，粒子の軌跡がまったく異なることがある。深層での動きに対して海嶺は大きな障壁となる。(ii) では，点源から一定の距離に達するまでの時間を，平均流速を使う場合とうずを含む流速を使う場合について求めて，その比を実測の流速データを用いた結果とくらべる。両者はよく一致する。